Comparative Evaluations of Frequency Response Analysis Methods for Fast and Precise Point-to-point Position Control

Yoshihiro Maeda
Department of Electrical and
Mechanical Engineering
Nagoya Institute of Technology
Gokiso, Showa, Nagoya 4668555
Email: ymaeda@nitech.ac.jp

Hiroki Tachibana
Department of Electrical and
Mechanical Engineering
Nagoya Institute of Technology
Gokiso, Showa, Nagoya 4668555
Email: h.tachibana.776@stn.nitech.ac.jp

Makoto Iwasaki
Department of Electrical and
Mechanical Engineering
Nagoya Institute of Technology
Gokiso, Showa, Nagoya 4668555
Email: iwasaki@nitech.ac.jp

Abstract—This paper examines frequency response analysis (FRA) methods using transient response signals in actual operation, for the fast and precise point-to-point position control of industrial servo systems. In industrial processing/manufacturing machines, the enormous fast and precise point-to-point trials are conducted with varieties of interval times, and parameter fluctuations of plants occur due to the self-heating, environment temperature variation, and aged deterioration. Therefore, FRA methods using the transient response signals in operation (e.g. force and position) are required to adaptation of controllers, stability analyses, and abnormal diagnoses. However, since initial and final values of the transient response signals are not the same in general in the point-to-point motion, it is difficult to analyze the accurate frequency characteristic of plant directly through the discrete Fourier transform (DFT)-based FRA. In this study, three practical FRA methods (windowing function, bandpass filter, and differentiator) are comparatively evaluated to examine the appropriate FRA method for the fast and precise servo systems. The comparative evaluations are conducted by experiments using a laboratory prototype galvano scanner.

I. INTRODUCTION

For industrial mechatronic systems such as electronics manufacturing/processing machines, industrial robots, machine tools, etc., fast and precise point-to-point positioning control is one of key technologies from viewpoints of high productivity and quality of products [1]. In order to realize the fine positioning performance, the two degree-of-freedom (2DoF) control is effective and widespread in the related research fields, and high-performance feedfoward (FF) and feedback (FB) controller designs as well as stability analyses are based on an accurate plant model [2]–[6].

The frequency response analysis (FRA) method sweeping sinusoidal signals (sine sweep) is widely used in industry to achieve the accurate plant model [7], [8]. The sine sweep method can analyze the frequency response with high signal-to-noise ratio in a wide frequency range. However, it is unfavorable to input the sinusoidal signals to the control system as a kind of disturbance when the target system are in operation of manufacturing and/or processing. Hence, in recent years, FRA methods which estimate the frequency characteristic of the plant with transient response signals in the operation have been actively studied [9]–[11]. The FRA methods estimate frequency responses based on the discrete Fourier transform (DFT), which requires a time-domain signal whose initial and final values are the same in order to obtain the accurate frequency-domain information. However, transient response signals (e.g., current, torque, position) in the point-to-point motion do not satisfy the condition in general. Although to apply windowing functions to the transient response signals is a general approach, it is impossible in theory to obtain the accurate plant characteristic from DFTs of the plant input and output.

In order to overcome this problem, the reference [12] proposed the band-pass filter (BPF)-based FRA scheme which performs pre-filtering for the original signals with BPFs. The BPF-based pre-filtering is highly simple and can obtain the accurate FRA result if the original response signals includes long enough steady states. However, in the industrial mechatronic systems, the point-to-point positioning trial is conducted repeatedly with short-interval time for reduction of the tact time. In such case, DFT might not work accurately since the steady state of the original signal was quite short.

This paper examines an improved FRA method using the transient response signals in operation for the fast and precise positioning motion with the short-interval time. In this study, a windowing function (hanning window) and a BPF [12] are introduced as conventional FRA methods, and each problem is clarified through theoretical examinations and experiments. In addition, a differentiator-based FRA method to overcome the problems in the conventional FRA methods is proposed. Comparative evaluations of the FRA methods are performed in experiments, by using a laboratory galvano scanner for industrial electronics processing machines.

II. GALVANO SCANNER AND ITS CONTROL SYSTEM

A. Galvano Scanner

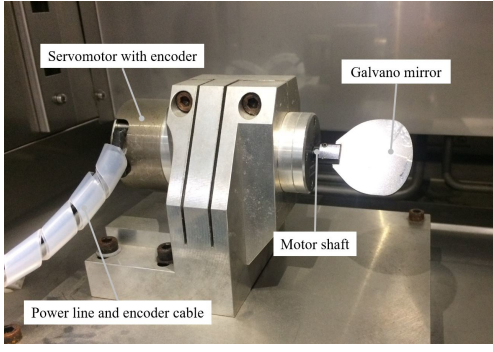Fig. 1 shows an external appearance of the laboratory galvano scanner for laser processing machines for printed

Fig. 1. External appearance of laboratory galvano scanner.

Fig. 2. Bode characteristics of plant.

Fig. 3. Response waveform of position and target control specification.

circuit boards. The galvano scanner is composed of a DC servomotor, a galvano mirror, and a rotary encoder (resolution of 1.49×10^{-6} rad/pulse). The servomotor is driven by the motor current i_m controlled by a servo amplifier, while the motor angle θ_m is directly detected by the encoder and is transferred to the servo controller. The servo controller with the sampling time of $T_s = 20$ μs outputs the motor current reference i_{ref} as the control input to the the servo amplifier. Hence, the target plant is handled as θ_m/i_{ref}. In order to realize high-quality and short-tact time processing, the fast and precise motion control of the galvano scanner is indispensable, which is one of key technologies to improve commercial competitiveness and develop innovative products.

B. Frequency Characteristic

Dotted lines in Fig. 2 denote a Bode plot of θ_m for i_{ref} which is measured by a sine sweep experiment. The galvano scanner has the primary resonant mode at 2.9 kHz, the second resonant mode at 6.1 kHz, other resonant modes in the higher frequency range over 10 kHz, and a phase delay property due to the servo amplifier. The resonant modes are caused by torsion of the motor shaft and deformation of the galvano mirror. A plant model $P(s) = \theta_m(s)/i_{ref}(s)$ considering the resonant modes up to $l = 2$ is mathematically formulated as

$$P(s) = e^{-Ls} K_g \left(\frac{1}{s^2} + \sum_{l=1}^{2} \frac{k_l}{s^2 + 2\zeta_l\omega_l s + \omega_l^2} \right), \quad (1)$$

where $K_g(= K_t K_c/J)$ is the gain with a combination of moment of inertia J, torque constant of motor K_t, and steady gain of the current control system K_c, ω_l is the natural angular frequency of l-th resonant mode, ζ_l is the damping coefficient, k_l is the resonant mode gain, and L is the equivalent dead time, respectively. Solid lines in Fig. 2 depict a Bode plot of $P(s)$. It has been experimentally confirmed that K_t and the resonant frequencies $f_1(= \omega_1/2\pi)$ and $f_2(= \omega_2/2\pi)$ fluctuate due to environment temperature, self heating, and aged deterioration [6]. Hence, the accurate FRA is required to identify the correct plant parameters for effective controller designs, stability analyses, and adaptation to the parameter fluctuation.
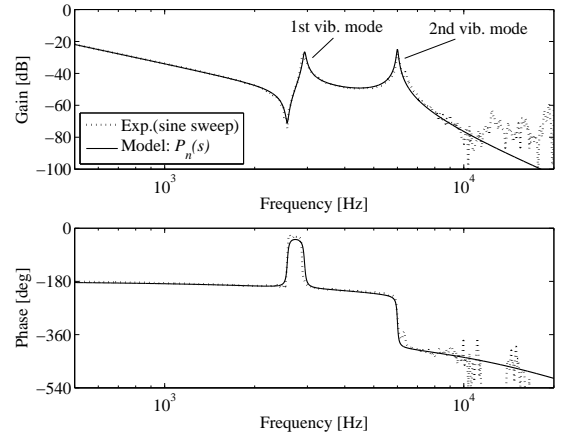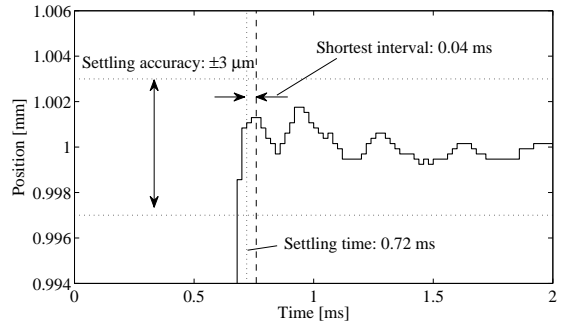
C. Target Control Specification

The typical control specification is defined as follows: the motor position (linear scale corresponding to the laser position) should follow the target position of $X_r = 1$ mm within the settling accuracy of ± 3 μm by the settling time of 0.72 ms($= 36T_s$) as shown in Fig. 3. Note that, in this study, the positioning trial is repeatedly performed with different interval times, considering actual operation of the galvano scanner. The shortest interval time which is defined as time between the target settling time in the previous motion and the next motion starting time is only 0.04 ms($= 2T_s$) for high productivity.

D. Point-to-point Position Control System

Fig. 4 shows a block diagram of the 2DoF position control system, where $C(z)$ is the FB controller composed of a phase lead/lag compensator and two notch filters [6], $P_n(z)$ is the discrete-time plant model of $P(s)$ in eq.(1) with a zeroth-order hold, u_{ff} is the FF control input, $u(= i_{ref})$ is the motor current reference as the control input, r is the target position trajectory reference, and $y(\propto \theta_m)$ is the motor position in linear scale, respectively. The FF control input $u_{ff}(z)$ is designed on the basis of the final-state control (FSC) framework with a plant model $P_n(z)$ so that y settles to the target position by the specified time of 0.72 ms. Since
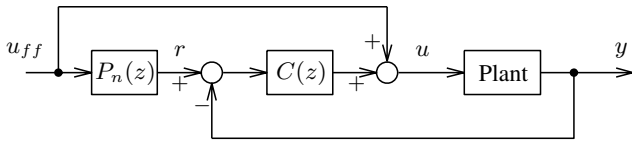
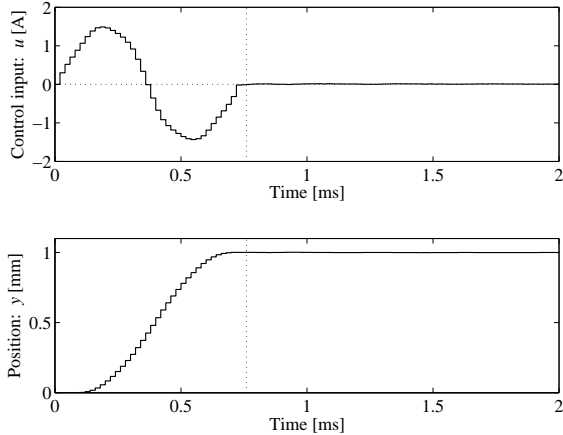Fig. 4. Block diagram of 2DoF position control system.

Fig. 5. Experimental response signals of control input and position.

Fig. 6. FRA system for transient response signals.

Fig. 7. Windowing function.

the FSC-based FF control is a model-based control manner, accurate $P_n(z)$ is necessary to achieve the desired positioning performance. In this study, the fast and repeatable positioning motion is conducted by using the 2DoF control system of Fig. 4, and u and y measured in each positioning trial as shown in Fig. 5 are utilized as the transient response signals for the FRA.

III. FRA METHODS

A. FRA System Using Transient Response Signals

A block diagram of the FRA system using the transient response signals in operation is shown in Fig. 6, where "DFT" is the DFT algorithm, $\widehat{P}(\omega)$ is the estimated frequency characteristic of the plant (FRA result), $F(z)$ is the pre-filter, u_f is the filtered input signal, y_f is the filtered output signal, $U_f(\omega)$ is the frequency characteristic of u_f, and $Y_f(\omega)$ is the frequency characteristic of y_f, respectively. In the FRA system enclosed by the dotted line, the original signals $u[i]$ and $y[i]$ at $t = iT_s$ ($i = 0, \ldots, N-1$) in operation (the interval time of NT_s) are input to $F(z)$ on-line, and the filtered signals $u_f[i]$ and $y_f[i]$ are transferred to the DFT algorithm. Here, the data length N_{dft} of DFT is set as $N_{dft} = 3800$ ($N < N_{dft}$) with consideration of the resolution of frequency (13.16 Hz). The time-domain data for DFT are defined as $\boldsymbol{u}_f = [u_f[0], u_f[1], \ldots, u_f[N-1], 0, \ldots, 0] \in R^{N_{dft}}$ and $\boldsymbol{y}_f = [y_f[0], y_f[1], \ldots, y_f[N-1], 0, \ldots, 0] \in R^{N_{dft}}$. Then, by using their frequency characteristics $U_f(\omega)$ and $Y_f(\omega)$, $\widehat{P}(\omega)$ is obtained as $\widehat{P}(\omega) = Y_f(\omega)/U_f(\omega)$.

Theoretically, it is required for DFT that initial and final values of a time-domain signal are the same (in this case, $u_f[0] = u_f[N-1] = 0$ and $y_f[0] = y_f[N-1] = 0$), since
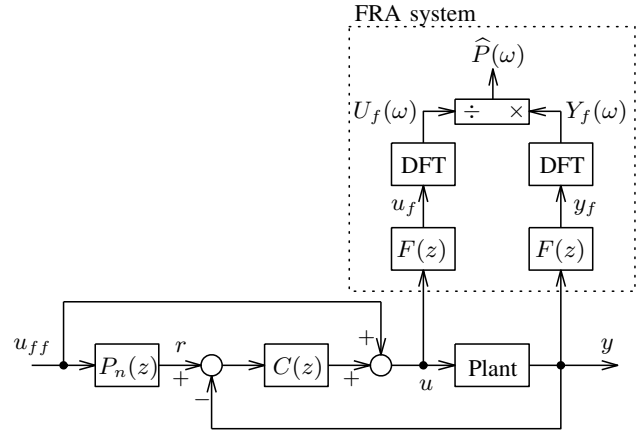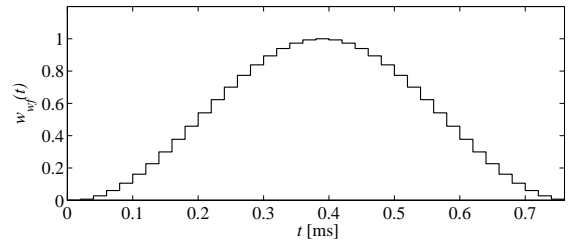
a discontinuity in the time-domain signal occurs undesired frequency components on the DFT result which does not exist in the original signal. However, in the point-to-point motion handled in this study, since the original signals (especially y) do not satisfy such condition as shown in Fig. 5, $\boldsymbol{u}_f$ and $\boldsymbol{y}_f$ might include the discontinuity. Therefore, in order to achieve accurate FRA result, the pre-filter $F(z)$ which suppresses the discontinuity in $\boldsymbol{u}_f$ and $\boldsymbol{y}_f$ is required.

B. Windowing Function-based FRA

The hanning window which is one of most popular windowing functions is introduced to suppresses the discontinuity in time-domain signals before DFT. The hanning window for a time-domain signal with the sampling time of T_s and the data length of N is mathematically formulated as

$$w_{wf}(t) = 0.5 \left(1 - \cos\frac{2\pi t}{NT_s} \right). \tag{2}$$

Fig. 7 shows the windowing function of eq.(2) in the case of $N = 38$. By multiplying eq.(2) to the original signal y as an example (i.e., $w_{wf}(t) \cdot y(t)$), the initial and final values of the filtered signals become zeros, and the discontinuity can be successfully suppressed. However, since the frequency characteristic of the filtered signal $Y_f(\omega)$ is expressed as convolution of $W_{wf}(\omega)$ and $Y(\omega)$ (i.e., $Y_f(\omega) = W_{wf}(\omega) * Y(\omega)$) in theory, the ratio of $Y_f(\omega)/U_f(\omega)$ does not equal to $Y(\omega)/U(\omega)$. Therefore, the windowing function-based FRA is not suitable for estimate of the plant frequency characteristic.
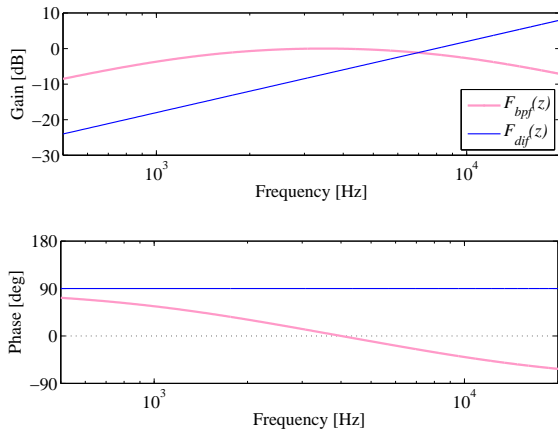
Fig. 8. Bode characteristics of band-pass filter and differentiator.

Fig. 9. Conceptual diagram of position response in absolutely integrable signal generation.

C. Band-pass Filter-based FRA [12]

The following band-pass filter with continuous-time expression is defined as the pre-filter $F(z)$ in Fig. 6, according to the reference [12].

$$F_{bpf}(s) = \frac{K_{bpf}s}{(s+\omega_l)(s+\omega_h)}, \tag{3}$$

where ω_l is the lower cutoff angular frequency, ω_h is the higher cutoff angular frequency, and K_{bpf} is the gain, respectively. ω_l and ω_h should be set appropriately so that the target frequency range to be estimated exists between ω_l and ω_h. In this study, ω_l and ω_h are set as $\omega_l = 2\pi \times 1500$ rad/s and $\omega_h = 2\pi \times 8000$ rad/s with consideration of the primary resonant mode at 2.9 kHz, while K_{bpf} is designed as $(\omega_l + \omega_h)/\omega_l\omega_h$. In the implementation, eq.(3) is discretized by Tustin transformation with the sampling time of T_s. Light solid lines in Fig. 8 depict the Bode plot of the discretized $F_{bpf}(z)$.

D. Differentiator-based FRA (Proposed Method)

A concept diagram of the proposed FRA method is shown in Fig. 9. A solid line denotes the time-domain position signal as the original signal $y_o[i] = y[i](i = 0, \ldots, N-1)$ in a point-to-point motion to the target position of X_r. Note that the next positioning motion starts at $t = NT_s$. In order to obtain the desired signal for DFT with the data length of $2N$, the proposed method connects y_o and the inversed original signal $-y_o$ as indicated by a dashed line. By using y_o, the connected signal $y_c[m]$ ($m = 0, \ldots, 2N-1$) is mathematically expressed as

$$y_c[m] = \begin{cases} y_o[m] & : m = 0, \ldots, N-1 \\ y_o[N-1] - y_o[m-N] & \\ & : m = N, \ldots, 2N-1 \end{cases}. \tag{4}$$

The frequency characteristic $Y_c(\omega)$ of eq.(4) is expressed as

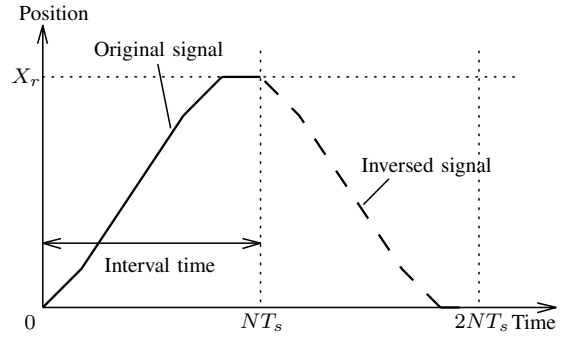$$Y_c(\omega) = \sum_{m=0}^{2N-1} y_c[m]e^{-j\omega mT_s}. \tag{5}$$

Here, the differential signal $y_c'[m]$ of $y_c[m]$ is defined as follows, by using y_c':

$$y_c'[m] = y_c[m] - y_c[m-1], \quad y_c[-1] = 0. \tag{6}$$

By substituting eq.(6) to eq.(5), $Y_c(\omega)$ can be expressed as

$$Y_c(\omega) = y_c'[0] + (y_c'[0] + y_c'[1])e^{-j\omega T_s} + \cdots$$
$$+ \sum_{m=0}^{2N-1} y_c'[m] \cdot e^{-j(2N-1)\omega T_s}. \tag{7}$$

In addition, y_c' satisfies the following equation from eq.(4).

$$y_c'[i] = -y_c'[i+N] \quad (i = 0, \ldots, N-1). \tag{8}$$

From eq.(7) and eq.(8), $Y_c(\omega)$ is reformulated as follows:

$$Y_c(\omega) = y_c'[0] \sum_{i=0}^{N-1} e^{-ji\omega T_s} + y_c'[1] \sum_{i=0}^{N-1} e^{-ji\omega T_s} + \cdots$$
$$+ y_c'[N-1] \sum_{i=0}^{N-1} e^{-ji\omega T_s}$$
$$= \sum_{i=0}^{N-1} y_c'[i]e^{-ji\omega T_s} \cdot \sum_{i=0}^{N-1} e^{-ji\omega T_s}. \tag{9}$$

Based on the above mathematical expression, the estimated frequency characteristic of plant $\widehat{P}(\omega) = Y_c(\omega)/U_c(\omega)$ calculated by using u_c and y_c is formulated as

$$\widehat{P}(\omega) = \frac{\sum_{i=0}^{N-1} y_c'[i]e^{-ji\omega T_s}}{\sum_{i=0}^{N-1} u_c'[i]e^{-ji\omega T_s}}. \tag{10}$$

Notice here, since the connected signals equal to the original signals at $i = 0, \ldots, N-1$ (i.e., $u_c[i] = u_o[i]$ and $y_c[i] = y_o[i]$), the numerator and the denominator of eq.(10) respectively express DFTs of the differential signals $u_o'[m]$ and $y_o'[m]$. Therefore, $\widehat{P}(\omega)$ satisfies the following equation.

$$\widehat{P}(\omega) = \frac{Y_c(\omega)}{U_c(\omega)} = \frac{Y_o'(\omega)}{U_o'(\omega)}. \tag{11}$$

Hence, to perform DFT for the connected signal as shown by Fig. 9 is theoretically equal to introduce the following differentiator $F_{dif}(z)$ as the pre-filter $F(z)$ in Fig. 6.
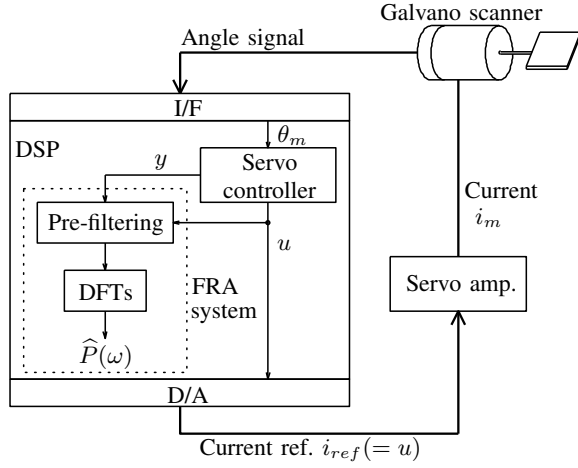
$$F_{dif}(z) = \frac{z-1}{z}. \tag{12}$$

Fig. 10. Configuration of experimental setup for galvano scanner control.

Fig. 11. Waveforms of filtered input and output in long-interval motion.

Fig. 12. FRA results in long-interval motion.

Dark solid lines in Fig. 8 show the Bode plot of $F_{dif}(z)$.

From the theoretical comparisons in Section III, it can be understood that the proposed FRA method is quite simple and easy to implement for online calculation, in comparison to the windowing function and BPF.

IV. COMPARATIVE EVALUATIONS OF FRA METHODS

A. Experimental Setup

Fig. 10 shows a configuration of an experimental setup for the galvano scanner control. The servo controller implemented on a DSP (System Design Service, Ltd., PDRS-6000) outputs the motor current reference $i_{ref}(= u)$ as the control input by using the detected position $\theta_m(\sim y)$ as input. The servo amplifier with the current control (control bandwidth of 20 kHz) drives the servomotor based on i_{ref}. The FRA system is also implemented on the DSP, and estimates the frequency characteristic of the plant $\widehat{P}(\omega)$ through the pre-filtering and DFTs for u and y. The sampling time of both the servo controller and the FRA system is $T_s = 20$ μs.

B. Evaluation in Long-interval Motion

Experiments of three FRA methods using the transient response signals are conducted for a long-interval positioning trial with the interval time of $NT_s = 2.0$ ms ($N = 100$). Fig. 11 shows response waveforms of the filtered signals u_f and y_f, while Fig. 12 shows FRA results of $\widehat{P}(\omega) = Y_f(\omega)/U_f(\omega)$. In both figures, dark dashed lines are the windowing function-based FRA method (WF), light solid lines are the BPF-based FRA method (BPF), and dark solid lines are the proposed differentiator-based FRA method (DIF), respectively. Here, the time-domain waveform of u_f generated by WF, u_f generated by DIF, and y_f generated by WF are displayed by increasing or decreasing their amplitude for comparison. In the case of WF, the FRA result includes remarkable errors for the actual plant characteristic of dark dotted lines measured by the sine sweep experiment, since the windowing function-based FRA method cannot obtain the accurate $\widehat{P}(\omega)$ in theory. On the other hand, in the cases of BPF and DIF, the filtered signals settle to zeros
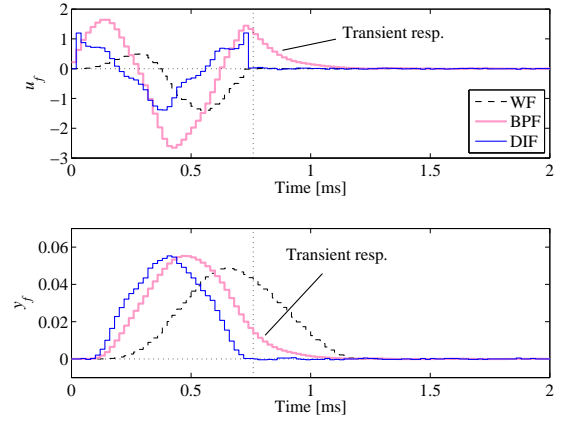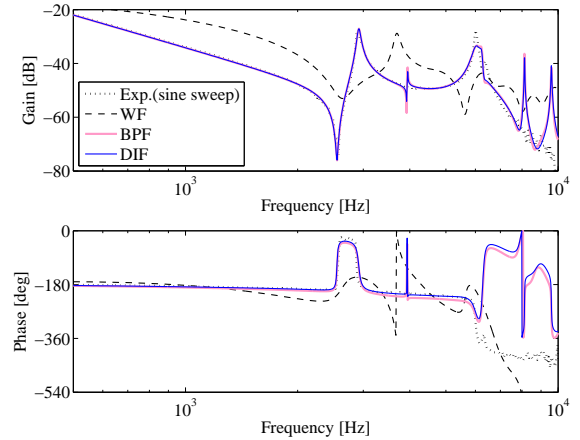
and show no discontinuity, while the FRA results successfully reproduce the rigid characteristic in the low frequency range less than 2.0 kHz and the primary resonant mode around 2.9 kHz of the actual plant. The steep errors in gain and phase appear at the same frequencies over 3.8 kHz, which are unavoidable phenomena in the DFT-based FRA. Notice that, in the case of BPF, since BPF of eq.(3) is defined as an infinite impulse response (IIR)-type filter, the filtered signals in Fig. 11 include transient responses after the settling time of 0.72 ms indicated by vertical dotted lines. Since the long-interval motion has enough steady state after 0.72 ms, the transient responses converges to zeros and does not include the discontinuity.

C. Evaluation in Short-interval Motion

Next, three FRA methods are experimentally applied to a short-interval positioning trial with the shortest interval time of $NT_s = 0.76$ ms ($N = 38$). Time-domain response waveforms of the filtered signals u_f and y_f are indicated in Fig. 13, while FRA results of $\widehat{P}(\omega) = Y_f(\omega)/U_f(\omega)$ are depicted in Fig. 14, respectively. The line properties are same as of Figs. 11 and 12. As same as of the long-interval motion in Section IV-A, WF
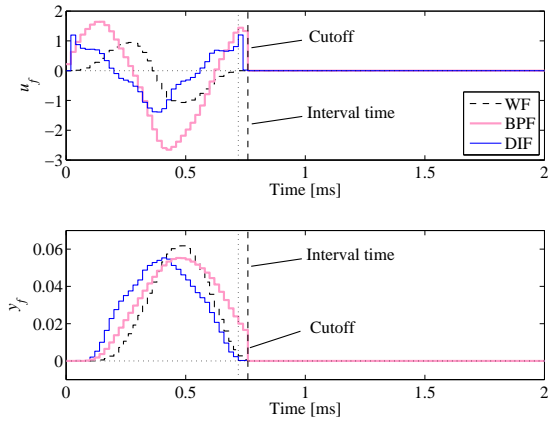
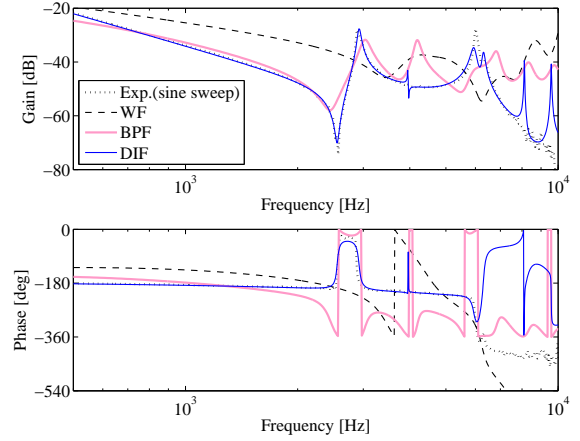Fig. 13. Waveforms of filtered input and output in short-interval motion.

Fig. 14. FRA results in short-interval motion.

cannot estimate the accurate FRA result due to the theoretical problem. In the case of BPF, since the filtered signals cannot converge to zeros until the interval time of 0.76 ms indicated by vertical dashed lines, the achievable time-domain signals u_f and y_f for DFT include the discontinuity at 0.76 ms due to cutoffs (becoming zeros) as shown in Fig. 13. As a result, $\widehat{P}(\omega)$ in Fig. 14 causes remarkable errors for the actual plant indicated by dark dotted lines in all frequencies. On the other hand, DIF does not cause the discontinuity and can achieve the accurate FRA result which is almost same as of the long-interval motion shown in Fig. 12.

It should be noted that resolution of input and output signals is an important index in the proposed FRA, since it has been confirmed that low resolution leads to deterioration of the FRA result. Hence, it is recommended to use high resolution sensors and controllers if possible or conduct signal processing to the input and output signals in order to prevent the influence of low resolution.

V. CONCLUSION

This paper has examined the FRA method using transient response signals in the fast and precise positioning motion, to achieve an accurate plant model for effective controller designs, adaptation to plant parameter fluctuations, analyses of stability, etc. In the DFT-based FRA, the pre-filtering which aims at generating time-domain signals suitable for DFT is necessary, and three pre-filters (i.e., windowing function, band-pass filter, and differentiator) are comparatively evaluated, especially focusing on their theoretical properties and transient responses of the filtered signals. From the series of experimental evaluations using a laboratory galvano scanner, the differentiator-based FRA method is most effective to estimate the accurate frequency characteristic of the plant, without regard to the interval time between previous and next positioning trials in repetitive operation.

As a future challenge, the differentiator-based FRA method will be applied to adaptive FF control for the plant parameter fluctuations due to self-heating and environment temperature variation.

REFERENCES

[1] M.-Y. Chen and J.-S. Lu, "High-precision motion control for a linear permanent magnet iron core synchronous motor drive in position platform," *IEEE Trans. Ind. Informat.*, vol. 10, no. 1, pp. 99–108, 2014.

[2] T. Atsumi, T. Arisaka, T. Shimizu, and H. Masuda, "Head-positioning control using resonant modes in hard disk drives," *IEEE/ASME Trans. Mechatronics*, vol. 10, no. 4, pp. 378–384, 2005.

[3] Y. Z. Tan and C. K. Pang, "On using Nyquist plots for relaxing convex conservative approximations in design of robust mechatronic systems," in *Proc. 7th IFAC Symposium Mechatron. Syst.*, pp. 115–119, 2016.

[4] H. Fujimoto, Y. Hori, and A. Kawamura, "Perfect tracking control based on multirate feedforward control with generalized sampling periods," *IEEE Trans. Ind. Electron.*, vol. 48, no. 3, pp. 636–644, 2001.

[5] M. Hirata, T. Hasegawa, and K. Nonami, "Seek control of hard disk drives based on final-state control taking account of the frequency components and the magnitude of control input," in *Proc. 7th Int. Workshop Advanced Motion Control*, pp. 40–45, 2002.

[6] Y. Maeda and M. Iwasaki, "Improvement of adaptive property by adaptive deadbeat feedforward compensation without convex optimization," *IEEE Trans. Ind. Electron.*, vol. 62, no. 1, pp. 466–474, 2015.

[7] S.-J. Kim and I.-J. Hz, "A frequency-domain approach to identification of mechanical systems with friction," *IEEE Trans. Automatic Control*, vol. 46, no. 6, pp. 888–893, 2001.

[8] Y.-Y. Chen, P.-Y. Huang, and J.-Y. Yen, "Frequency-domain identification algorithms for servo systems with friction," *IEEE Trans. Control Syst. Tech.*, vol. 10, no. 5, pp. 654–665, 2002.

[9] Y. Matsui, H. Ayano, and K. Nakano, "Parametric plant modeling using one-shot closed-loop transient response data," in *Proc. 11th Int. Conf. Electrical Eng./Electronics, Computer, Telecommunications and Information Technology*, pp. 1–6, 2014.

[10] H. Sekine, S. Ueda, and M. Hirata, "System identification of a galvano scanner using input-output data obtained from positioning control," in *Proc. 2015 European Control Conf.*, pp. 1297–1302, 2015.

[11] S. Masuda, M. Kano, and Y. Yasuda, "A fictitious reference iterative tuning method with simultatenous delay parameter tuning of the reference model," in *Proc. Int. Conf. Networking, Sensing and Control*, pp. 422–427, 2009.

[12] Y. Matsui, T. Kimura, and K. Nakano, "Plant model analysis based on closed-loop step response data," in *Proc. IEEE Int. Conf. Control Applications*, pp. 677–682, 2010.